OPTICS

Infrared electric field sampled frequency comb spectroscopy

Abijith S. Kowligy[1,2*†], Henry Timmers[1*], Alexander J. Lind[1,2*], Ugaitz Elu[3], Flavio C. Cruz[1,4], Peter G. Schunemann[5], Jens Biegert[3,6], Scott A. Diddams[1,2†]

Probing matter with light in the mid-infrared provides unique insight into molecular composition, structure, and function with high sensitivity. However, laser spectroscopy in this spectral region lacks the broadband or tunable light sources and efficient detectors available in the visible or near-infrared. We overcome these challenges with an approach that unites a compact source of phase-stable, single-cycle, mid-infrared pulses with room temperature electric field–resolved detection at video rates. The ultrashort pulses correspond to laser frequency combs that span 3 to 27 μm (370 to 3333 cm^{-1}), and are measured with dynamic range of $>10^6$ and spectral resolution as high as 0.003 cm^{-1}. We highlight the brightness and coherence of our apparatus with gas-, liquid-, and solid-phase spectroscopy that extends over spectral bandwidths comparable to thermal or infrared synchrotron sources. This unique combination enables powerful avenues for rapid detection of biological, chemical, and physical properties of matter with molecular specificity.

INTRODUCTION

The resonant interaction of infrared light with matter provides rich structural and functional information in complex biological (*1*, *2*), chemical (*3*–*5*), and physical systems (*6*, *7*). Notable examples include studying conformational changes in proteins (*8*, *9*), tracking chemical and ultrafast dynamics (*10*–*13*), measuring vibrational spectra with high resolution (*14*, *15*), and exploring the origins of chirality (*16*, *17*). Light sources with full mid-infrared (MIR; 3 to 25 μm) coverage that simultaneously address multiple molecular vibrational modes with user-specified spectral and temporal resolution are beneficial for all these applications, as well as the growing field of infrared spectro-imaging (*18*–*20*). Owing to the disparate and demanding criteria (e.g., brightness, bandwidth, and resolution), existing technologies such as thermal sources, synchrotrons, tunable lasers [quantum cascade and semiconductor lasers (*21*, *22*)], and parametric oscillators (*23*, *24*) often lack the desired properties or become increasingly complex. Adding to this complexity, infrared photodetection requires cryogenic cooling for low-noise operation and exhibits poor quantum efficiencies above 12 μm. In this work, we introduce a simple yet general framework for the generation of coherent MIR light spanning 3 to 27 μm and direct electric field detection of the corresponding near–single-cycle pulses. Complete infrared electric field readout at video rates using room temperature near-infrared (NIR) photodetectors resolves millions of phase-locked frequency comb modes that comprise the infrared spectrum. We highlight these advantages in precision spectroscopy of ammonia (*25*, *26*) and carbon dioxide (*27*) with simultaneous spectral coverage and resolution not achieved with other laser sources. Moreover, with brightness and scan-free acquisition rates 100 times greater than found in conventional Fourier transform spectrometers, our approach provides increased sensitivity and speed in recording the full infrared spectra of biological and molecular compounds in the condensed phase.

EXPERIMENTAL SYSTEM

In our experimental system, intra-pulse difference-frequency generation (DFG) in quadratic nonlinear media provides a simple and robust source of ultrashort infrared pulses with an intrinsically stable carrier-envelope phase (CEP) (*28*, *29*). The corresponding multi-octave instantaneous bandwidth allows us to probe multiple ro-vibrational excitations from 500 to 2500 cm^{-1}. Leveraging the CEP stability, we implement dual frequency comb electro-optic sampling (EOS) (Fig. 1A), which directly measures the MIR electric field and removes the need for cryogenically cooled photodetectors. In dual-comb EOS, the electric field of the MIR pulse train (with repetition rate $f_r + \Delta f_r$) is sampled by sum-frequency (SF) mixing with an NIR few-cycle pulse train (with repetition rate f_r). The nonlinear interaction results in an infrared field–dependent polarization rotation of the sampling pulse that is resolved via ellipsometry using room temperature InGaAs photodetectors (Fig. 1A) (*30*, *31*). Because of the repetition rate offset, the sampling pulse scans across the MIR electric field automatically and a complete electric field measurement is made every $\Delta f_r^{-1} \simeq 20$ ms.

Dual-comb sampling of radiation (also known as asynchronous optical sampling) has been used in the terahertz domain (optical period, $\tau_{THz} \simeq 1$ ps) using >50-fs-long optical pulses (*32*, *33*). However, its extension to the MIR has been limited by the required subcycle timing jitter and few-cycle sampling pulses (<10 fs). We overcome these challenges and measure a mutual timing jitter of 80 as between the two frequency combs, corresponding to <20-mrad residual phase noise for a 10-μm field. This exacting criterion is seen intuitively in the frequency domain, where the nonlinear sampling results in a new SF comb, with the entire MIR spectrum folded into each free spectral range (Fig. 1B) (*34*, *35*). Thus, coherent multiheterodyne beating occurs in the NIR, with the sampling pulse serving as a local oscillator comb.

Applications of EOS in the MIR, including sensitive spectroscopy, have been shown previously (*30*, *31*, *36*–*38*). However, previous measurements in the MIR used a mechanical translation stage to vary the time delay, restricting the resolution and acquisition time to

[1]Time and Frequency Division, NIST, Boulder, CO 80305, USA. [2]Department of Physics, University of Colorado, Boulder, CO 80305, USA. [3]ICFO - Institut de Ciencies Fotoniques, The Barcelona Institute of Science and Technology, 08860 Castelldefels (Barcelona), Spain. [4]Instituto de Fisica Gleb Wataghin, Universidade Estadual de Campinas, Campinas, São Paulo 13083-859, Brazil. [5]BAE Systems, Nashua, NH 03060, USA. [6]ICREA, Pg. Lluis Companys 23, 08010 Barcelona, Spain.
*The authors contributed equally to this work.
†Corresponding author. Email: abijith.kowligy@gmail.com (A.S.K.); scott.diddams@nist.gov (S.A.D.)

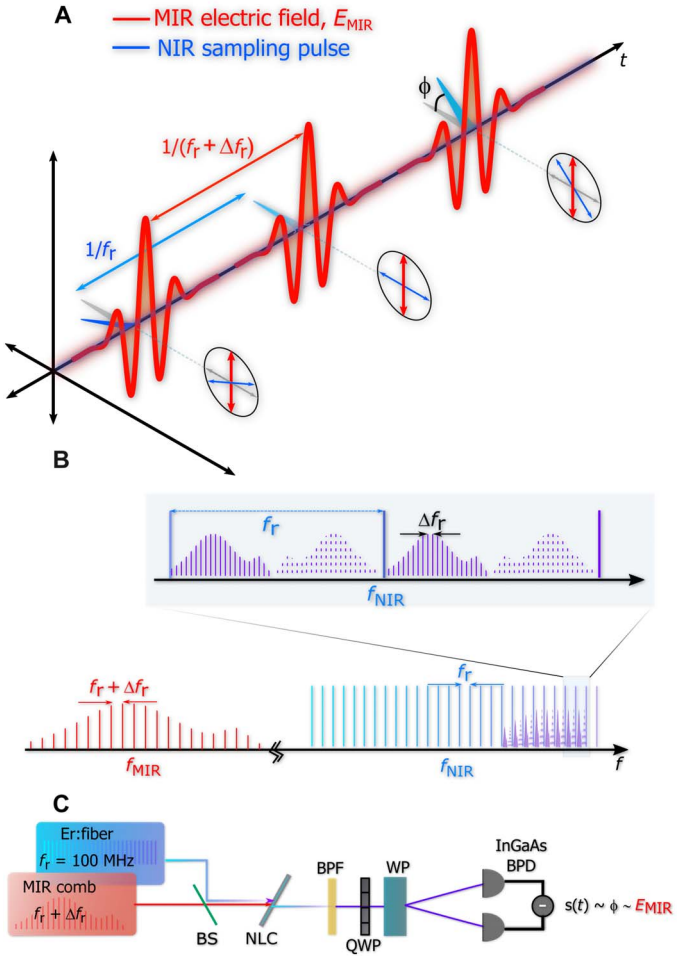

Fig. 1. Infrared dual frequency comb electric field sampling. (**A**) An MIR electric field (with repetition rate $f_r + \Delta f_r$) induces a nonlinear polarization rotation, ϕ, on an NIR sampling pulse (with repetition rate f_r) that is directly proportional to its amplitude, E_{MIR}. (**B**) In the frequency domain, the entire MIR spectrum is down-sampled to Δf_r and folded into the free-spectral range of the NIR sampling pulse such that it is contained within every Nyquist zone ($f_r/2$). (**C**) Experimentally, the sampling and MIR pulses are combined at a germanium beam splitter (BS), and the SF interaction occurs in an electro-optic crystal (NLC). The output is spectrally filtered with a bandpass filter (BPF). Ellipsometry using a quarter waveplate (QWP), Wollaston prism (WP), and balanced photodetectors (BPD) yields a signal, $s(t) \propto E_{MIR}$.

wave number and second scales, respectively. In our experiment, the MIR light and the NIR sampling pulse are derived from two mutually phase-locked 100-MHz repetition rate erbium fiber lasers that produce few-cycle pulses (Fig. 1C) (*29*). This scan-free implementation avoids mechanically induced stepping and jitter errors while providing high spectral resolution (0.003 cm^{-1}), intrinsic and absolute frequency calibration ($\Delta f/f < 10^{-12}$), and millisecond time scale acquisition. Using a <10-fs NIR pulse, the MIR electric field is sampled in a gallium selenide (GaSe) crystal, with a time-domain signal-to-noise ratio (SNR) exceeding 10^4 in 20 min of averaging, corresponding to a single-shot SNR ~ 40 in a 50-MHz electrical bandwidth (Fig. 2A).

RESULTS

The MIR laser frequency combs are generated in three nonlinear crystals, namely, periodically poled lithium niobate (PPLN), orientation-patterned gallium phosphide (OP-GaP), and GaSe, providing spectral coverage from 3 to 27 μm (Fig. 2B). For the MIR comb generated in OP-GaP, the anomalous dispersion from crystal propagation is compensated by the normal dispersion from the germanium beam splitter, resulting in a near–single-cycle oscillation (Fig. 2A). The MIR pulse is 1.2 cycles in duration, corresponding to 29 fs, and is coherently recorded with a temporal dynamic range of 10^6. The demonstrated phase-stable single-cycle transients are also desirable for seeding amplifier systems in high-harmonic generation experiments (*39*), for studying phase-sensitive photoemission (*40*), and for multidimensional vibrational spectroscopy (*41*).

Following the Fourier transform of the measured electric field transient, we use the resolved frequency comb teeth to perform accurate, high-resolution, broadband spectroscopy across the spectral range of 500 to 3000 cm^{-1}. The multi-octave instantaneous bandwidth we achieve is unparalleled when compared to other frequency comb sources (*24*, *42*, *43*) and enables simultaneous probing of multiple vibrational bands without the need for tuning. Figure 2B shows the absorption signatures of important compounds for atmospheric chemistry such as methane, ethane, carbon dioxide, and water vapor in both the functional group (1500 to 4000 cm^{-1}) and molecular fingerprint regions (500 to 1500 cm^{-1}). In particular, the vibrational spectra of the P, Q, and R branches of the O—C—O bending vibration of CO_2 around 15 μm are measured using the OP-GaP MIR comb over a 2-m path length (Fig. 2C). Comparison with a model (*44*) shows that quantitative results are not limited by our dual-comb EOS detection. The intensity and phase of the absorption lines, which are pressure-broadened to 5 GHz, are resolved with individual comb teeth of the frequency comb (Fig. 2C). The comb teeth are stabilized to a 10-kHz level, which is not a fundamental limit, but represents the instrument line shape in our present spectrometer (*45*). With time-domain apodization of the electric field signal, 500-MHz resolution data are also shown, which exhibit higher SNR by a factor of $\sqrt{5}$ (Fig. 2D).

Ammonia is an important compound used in the agricultural and biopharmaceutical industries (*26*) and fundamental scientific studies including astrochemistry (*7*). In Fig. 3, we present our measurement of its ν_2 vibration (A_1 symmetric bend) across 770 to 1165 cm^{-1} (8.6 to 13 μm), where 118,000 comb teeth are individually resolved. Similar simultaneous spectral coverage has only previously been achieved with thermal sources (*46*) and scanning Fourier transform spectrometers, but here, we additionally leverage the intrinsic frequency accuracy and resolution that the frequency comb provides. Excellent agreement with the HITRAN model (*44*) is seen across the entire spectrum. We observe the splitting in the *Q* branch due to pyramidal inversion of the NH_3 molecule, where the nitrogen atom undergoes room temperature quantum tunneling through the potential barrier formed by the H_3 plane (*47*). The combination of the broadband high-resolution spectroscopy and room temperature photodetection renders our system powerful for studying quantum chemistry (*48*), interstellar composition (*25*), and mapping individual crystalline domains in nanoscale materials (*49*).

An advantage of our approach is that it provides full and simultaneous MIR spectral coverage at a user-defined resolution. Here, we use numerical apodization to yield resolution that is more appropriate for broadband condensed phase samples, but high-repetition rate frequency combs (*50*) or dynamic repetition rate switching (*51*) can be used to tailor the resolution and further increase data acquisition rates. We demonstrate these advantages with broadband liquid-phase absorption signatures of an *R*-(−)-carvone, a prototypical chiral molecule,

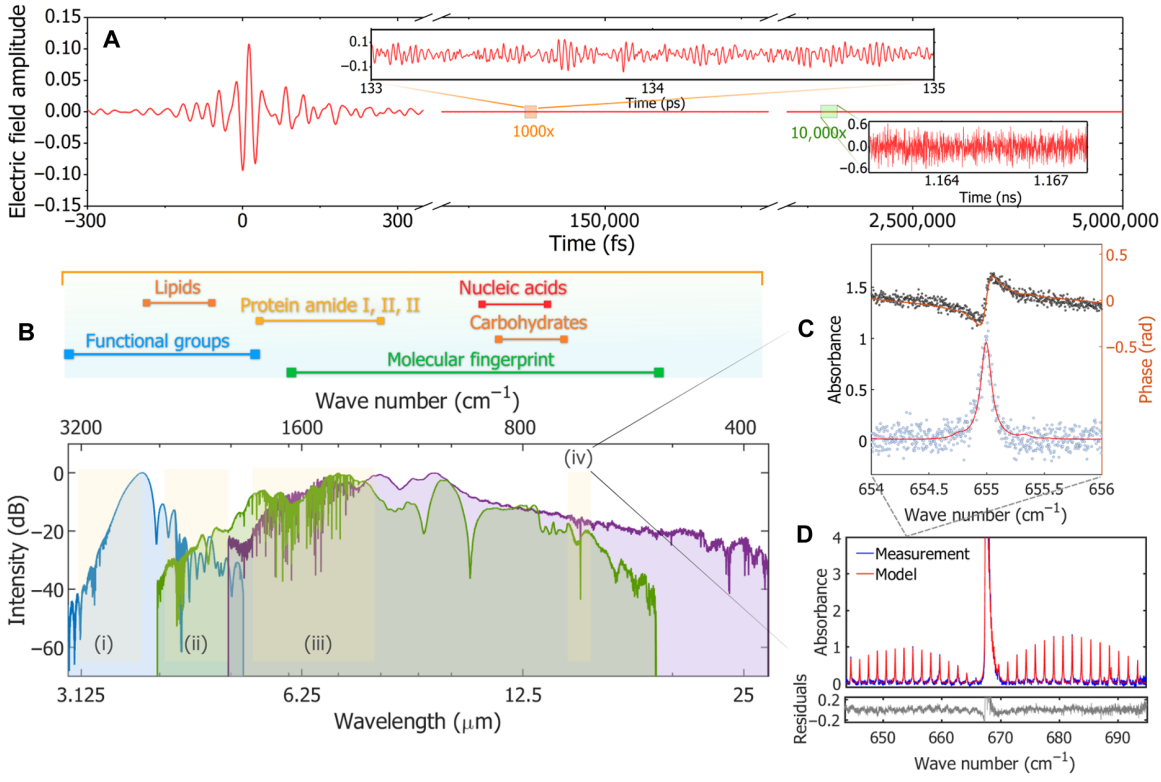

Fig. 2. MIR electric field measurements with high dynamic range. (**A**) A 1.2-cycle MIR electric field, oscillating at 7.6 μm (39 THz, 1316 cm^{-1}), is sampled with a 5-fs resolution. The dual frequency comb measurement enables observation of the trailing molecular free induction decay of atmospheric absorbents, e.g., H_2O at 135 ps away from the centerburst (inset, top). The noise level is 10,000 times smaller than the signal with 22 min of averaging (inset, bottom). (**B**) Ultrabroadband MIR spectra corresponding to the Fourier transform of the measured electric fields from PPLN (blue), OP-GaP (green), and GaSe (purple)—encompassing the functional group and molecular fingerprint regions and facilitating the study of important organic compounds such as proteins. Vibrational spectra of (i) C–H stretches in CH_4 and C_2H_6, (ii) anti-symmetric C–O stretch in CO_2, (iii) O–H–O bend in H_2O, and (iv) O–C–O bend in CO_2 are all seen. (**C**) Comb-tooth resolution measurement (blue) of a single absorption feature in the R branch is compared against the modeled spectrum (red) for the ν_2 vibration (symmetric O–C–O bend) of CO_2. (**D**) The absorption of this CO_2 bending mode is shown from 630 to 700 cm^{-1} at a 500-MHz resolution. The residuals (gray) show quantitative agreement with the model.

and the amide vibrations in a monoclonal antibody (NISTmAb), a reference for the biopharmaceutical industries (Fig. 4). In Fig. 4A, liquid-phase absorption spectra acquired over two octaves from 500 to 2500 cm^{-1} are shown, with the ν_2 (O—H—O bend) vibration at 1650 cm^{-1} being saturated. In Fig. 4B, the absorption signature of a dried NISTmAb film is shown from the 1200- to 1800-cm^{-1} region that identifies the amide I, II, and III bands. The amide bands in proteins are used to determine the folding, unfolding, and aggregating mechanisms (*8*, *52*, *53*). The center frequencies of the amide I (1636 cm^{-1}) and amide II bands (1549 cm^{-1}) indicate a β-sheet structure for the protein, agreeing with previous studies (*8*, *54*).

CONCLUSION

In conclusion, we presented a comprehensive framework for MIR laser spectroscopy that unified the highly desired qualities of phase-stable single-cycle temporal waveforms and ultrabroadband spectral coverage with room temperature, video rate, electric field detection with bandwidth extending from 370 to 3333 cm^{-1}. Inheriting the robustness and simplicity from the NIR pulses derived from erbium fiber lasers, the compact source provides a benchtop (<0.5 m^2) footprint for infrared spectroscopy in the molecular fingerprint region and beyond. Quantitative high-resolution spectroscopy is demonstrated with electric field sampling in a spectral region beyond the reach of high-speed HgCdTe detectors. In addition to probing narrow linewidth transitions in gas phase, we probe wave number–scale transitions in liquid- and solid-state materials across 500 to 2500 cm^{-1} and capture both functional group and molecular fingerprint regions. Such broadband spectroscopy is critical for strongly coupled interactions between infrared light and condensed phase matter that enable applications such as quantum computation within the internal degrees of freedom in a molecule (*55*). When combined with novel imaging techniques such as infrared atomic force microscopy and scanning scattering near-field optical microscopy, the system described here would enable nanoscale spectro-imaging of samples that currently require the bandwidth and brightness of a synchrotron. Last, the near–single-cycle nature of our MIR light source can serve as a robust seed for parametric amplifiers in strong-field physics (*56*).

MATERIALS AND METHODS

Phase locking

We used two self-referenced Er:fiber lasers with nominal repetition rate, f_r = 100 MHz, to generate the MIR light and sampling pulse for dual-comb EOS. The lasers were made mutually coherent by optical phase locking each one to a cavity-stabilized continuous-wave laser at 1550 nm. The absolute linewidths of the frequency combs were tied to

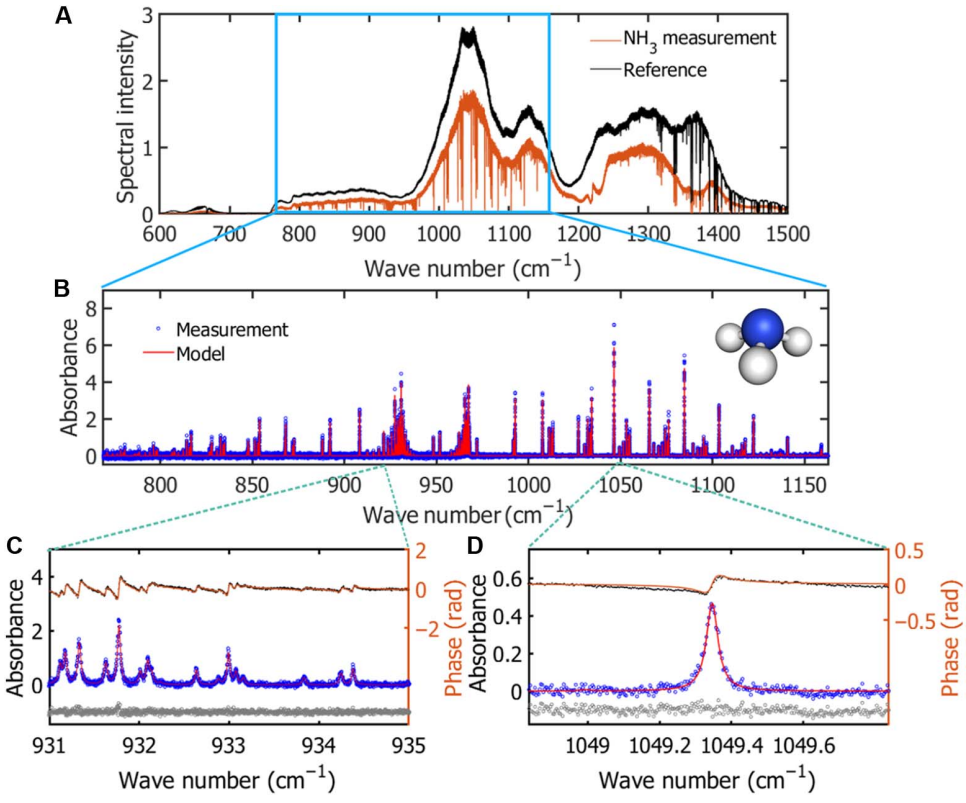

Fig. 3. High-resolution and broad bandwidth spectroscopy of ammonia. (**A**) Absorption measurements are performed with instantaneous octave-spanning bandwidth from 600 to 1500 cm^{-1} (6.7 to 16.7 μm) in ambient conditions. (**B**) The ν_2 vibration (A_1 symmetric bend) of gas-phase ammonia is measured (blue) between 770 and 1160 cm^{-1} (8.6 to 13 μm) with a resolution of 0.0033 cm^{-1} and compared to modeled absorption (red). The averaging time was 88 min. (**C**) and (**D**) Quantitative agreement is seen across the entire spectrum for both intensity and phase. The line intensity residuals (gray) are shown offset from zero on the same scale.

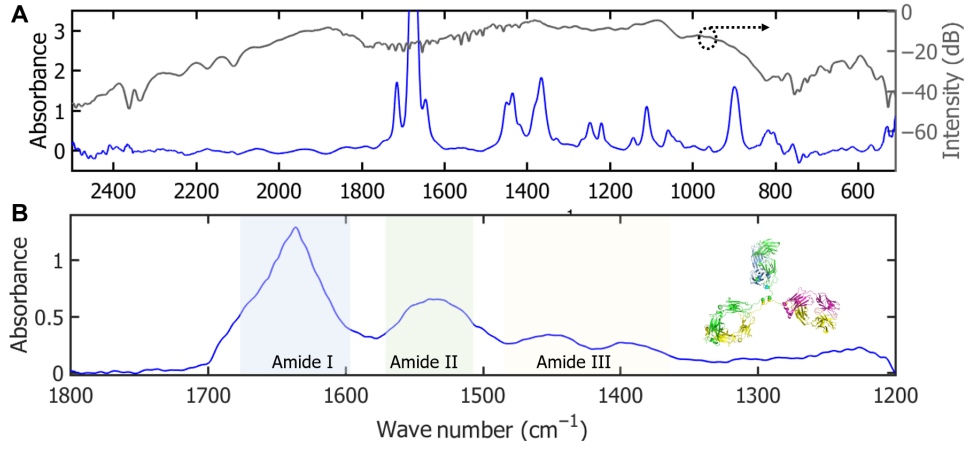

Fig. 4. Broadband condensed phase absorbers across 500 to 2500 cm^{-1}. (**A**) Liquid-phase R-(-)- carvone over a 15-μm path length is measured at a resolution of 1.2 cm^{-1}. The reference spectrum is shown on the right axis (in logarithmic scale). (**B**) Infrared absorption spectrum (with a resolution of 4 cm^{-1}) of the monoclonal antibody, NISTmAb, showing the amide I, II, and III bands. The β-sheet structure is shown graphically in the inset.

the 10-kHz linewidth of the continuous-wave laser. The line-position accuracy of the comb modes is 10^{-12}, which is given by the precision with which we measured the lasers' repetition rates. While appropriate for the spectroscopy shown here, these are not fundamental limits, and sub-hertz linewidths and uncertainties below 10^{-15} can be implemented if required. Moreover, while single-measurement resolution of 100 MHz (0.003 cm^{-1}) is shown here, by stepping the repetition rates of the combs, the modes of the combs could be continuously swept across the full 100-MHz free-spectral range, thereby providing resolution down to the comb-tooth linewidth (*57*). Locking was achieved via feedback to the laser that was provided using a combination of an intra-cavity electro-optic modulator at a 1-MHz bandwidth and a piezo-electric transducer at a 10-Hz bandwidth. The integrated residual optical phase noise is ~100 mrad, corresponding

to a relative timing jitter of 83 as. In this work, Δf_r is in the range of 40 to 50 Hz. However, we verified coherent averaging at Δf_r = 15 Hz, corresponding to a 1.5-fs timing resolution.

Few-cycle NIR pulse synthesis

A nonlinear amplification scheme in erbium-doped fiber, followed by spectral broadening in normal-dispersion highly nonlinear fiber, provides the bandwidth for a 10-fs NIR pulse that is compressed in bulk fused silica. Residual third-order dispersion was compensated using a pair of chirped mirrors. Frequency-resolved optical gating (FROG) was used to measure the pulse duration.

MIR generation

The few-cycle pulse was focused into a quadratic nonlinear crystal using an off-axis parabolic mirror (f = 25 mm) to drive intra-pulse DFG and produce MIR light. We generated light from 3- to 5.5-μm light in a 1-mm-thick PPLN with power ranging from 500 μW to 1.2 mW. In OP-GaP, a 1-mm-thick fanout crystal with grating periods in the range of 50 to 65 μm was used to generate broadband long-wave infrared light. The spectrum spanning 4 to 20 μm was generated in a 63-μm grating period and corresponded to 100 to 200 μW. The center frequency of the spectrum was determined by calculating its center of mass after deconvolving the spectrum using the response function. In a 500-μm-thick GaSe, type II phase matching was used, and the broadband spectrum provided approximately 2 μW across the entire band.

EOS detection

The SF generation (SFG) from the electro-optic crystal was filtered using a 25- or 50-nm bandpass filter around 1300 nm and analyzed using a broadband quarter waveplate followed by a high-extinction Wollaston prism. The light was focused onto a commercial InGaAs balanced photodetector (BPD). The differential photocurrent, $\Delta I/I \propto \Delta n \propto (d_{\mathrm{eff}}/n_0)E_{\mathrm{MIR}}$, is proportional to the SFG-induced refractive index change (or, equivalently, nonlinear phase shift) (*58*). d_{eff} is the frequency-dependent second-order susceptibility of the electro-optic crystal, n_0 is the refractive index of the NIR carrier frequency in GaSe, and E_{MIR} is the MIR electric field. For the near–single-cycle OP-GaP MIR output, based on a focused beam waist of 100 μm^2 and a pulse duration of 30 fs with an average power of 100 μW, we estimated that the peak electric field in the GaSe crystal is E_{MIR} = 15 kV/cm. To trigger the dual-comb readout at the 50-Hz refresh rate, we used a nonlinear cross-correlation signal acquired via SFG between the two few-cycle NIR pulses in a 1-mm-thick barium borate crystal that was detected with a Si avalanche photodiode.

EOS response function

Although the temporal increment in the dual-comb EOS configuration is ≈5 fs (Δf_r = 50 Hz), the finite pulse duration of the sampling pulse (10 fs) imposes an instrument response that must be removed by deconvolution to attain the true electric field waveform of the infrared radiation. As this measurement can be considered a convolution in time domain, the "true" electric field may be acquired by deconvolving the response function of EOS (*59*, *60*). The electric field of the SFG is proportional to the envelope of the NIR sampling pulse, i.e., $E_{\mathrm{SFG}} \propto d_{\mathrm{eff}} \frac{\exp[i\Delta kL]-1}{i\Delta k} \times E_{\mathrm{NIR}}E_{\mathrm{MIR}}$, $\Delta k = \frac{1}{c}(n(\omega_{\mathrm{MIR}})\omega_{\mathrm{MIR}} - n_g(\omega_{\mathrm{MIR}})\omega_{\mathrm{NIR}})$ is the phase mismatch in the SFG process, and E_{NIR} is the sampling pulse envelope. By computing the phase mismatch and acquiring E_{NIR} via FROG, a response function can be constructed (fig. S1). Deconvolving in the frequency domain, and inverse Fourier transforming the spectrum, provides the electric field measurement without the influence of the finite pulse duration in the sampling pulse. Because we operated far from phonon resonances in GaSe, d_{eff} was taken to be frequency independent. The phase-matching curves for the 30-μm-thick EOS crystal at two different angles are shown in fig. S3. The phase-matching bandwidth is factored into the EOS response function, and it is directly proportional to the sampling efficiency (fig. S1).

SUPPLEMENTARY MATERIALS

Supplementary material for this article is available at http://advances.sciencemag.org/cgi/content/full/5/6/eaaw8794/DC1

Section S1. Noise in EOS detection
Section S2. Noise-equivalent absorption in dual-comb EOS
Section S3. Atmospheric water vapor in the 585- to 630-cm^{-1} band
Fig. S1. EOS response function.
Fig. S2. Atmospheric water vapor absorption in the 585- to 630-cm^{-1} band.
Fig. S3. Phase-matching curves for SFG in GaSe.
Reference (*61*)

REFERENCES AND NOTES

1. D. C. Fernandez, R. Bhargava, S. M. Hewitt, I. W. Levin, Infrared spectroscopic imaging for histopathologic recognition. *Nat. Biotechnol.* **23**, 469–474 (2005).
2. G. Bellisola, C. Sorio, Infrared spectroscopy and microscopy in cancer research and diagnosis. *Am. J. Cancer Res.* **2**, 1–21 (2011).
3. C. Brif, R. Chakrabarti, H. Rabitz, Control of quantum phenomena: Past, present and future. *New J. Phys.* **12**, 075008 (2010).
4. J. Kirkby, J. Curtius, J. Almeida, E. Dunne, J. Duplissy, S. Ehrhart, A. Franchin, S. Gagné, L. Ickes, A. Kürten, A. Kupc, A. Metzger, F. Riccobono, L. Rondo, S. Schobesberger, G. Tsagkogeorgas, D. Wimmer, A. Amorim, F. Bianchi, M. Breitenlechner, A. David, J. Dommen, A. Downard, M. Ehn, R. C. Flagan, S. Haider, A. Hansel, D. Hauser, W. Jud, H. Junninen, F. Kreissl, A. Kvashin, A. Laaksonen, K. Lehtipalo, J. Lima, E. R. Lovejoy, V. Makhmutov, S. Mathot, J. Mikkilä, P. Minginette, S. Mogo, T. Nieminen, A. Onnela, P. Pereira, T. Petäjä, R. Schnitzhofer, J. H. Seinfeld, M. Sipilä, Y. Stozhkov, F. Stratmann, A. Tomé, J. Vanhanen, Y. Viisanen, A. Vrtala, P. E. Wagner, H. Walther, E. Weingartner, H. Wex, P. M. Winkler, K. S. Carslaw, D. R. Worsnop, U. Baltensperger, M. Kulmala, Role of sulphuric acid, ammonia and galactic cosmic rays in atmospheric aerosol nucleation. *Nature* **476**, 429–433 (2011).
5. B. Nozière, M. Kalberer, M. Claeys, J. Allan, B. D'Anna, S. Decesari, E. Finessi, M. Glasius, I. Grgić, J. F. Hamilton, T. Hoffmann, Y. Iinuma, M. Jaoui, A. Kahnt, C. J. Kampf, I. Kourtchev, W. Maenhaut, N. Marsden, S. Saarikoski, J. Schnelle-Kreis, J. D. Surratt, S. Szidat, R. Szmigielski, A. Wisthaler, The molecular identification of organic compounds in the atmosphere: State of the art and challenges. *Chem. Rev.* **115**, 3919–3983 (2015).
6. C. Lemarchand, M. Triki, B. Darquié, C. J. Bordé, C. Chardonnet, C. Daussy, Progress towards an accurate determination of the Boltzmann constant by Doppler spectroscopy. *New J. Phys.* **13**, 073028 (2011).
7. P. T. P. Ho, C. H. Townes, Interstellar ammonia. *Annu. Rev. Astron. Astrophys.* **21**, 239–270 (1983).
8. A. Barth, Infrared spectroscopy of proteins. *Biochim. Biophys. Acta* **1767**, 1073–1101 (2007).
9. J. E. Katon, Infrared microspectroscopy. A review of fundamentals and applications. *Micron* **27**, 303–314 (1996).
10. A. J. Fleisher, B. J. Bjork, T. Q. Bui, K. C. Cossel, M. Okumura, J. Ye, Mid-infrared time-resolved frequency comb spectroscopy of transient free radicals. *J. Phys. Chem. Lett.* **5**, 2241–2246 (2014).
11. M. Thämer, L. D. Marco, K. Ramasesha, A. Mandal, A. Tokmakoff, Ultrafast 2D IR spectroscopy of the excess proton in liquid water. *Science* **350**, 78–82 (2015).
12. T. L. Cocker, V. Jelic, M. Gupta, S. J. Molesky, J. A. J. Burgess, G. D. L. Reyes, L. V. Titova, Y. Y. Tsui, M. R. Freeman, F. A. Hegmann, An ultrafast terahertz scanning tunnelling microscope. *Nat. Photonics* **7**, 620–625 (2013).
13. T. Rybka, M. Ludwig, M. F. Schmalz, V. Knittel, D. Brida, A. Leitenstorfer, Sub-cycle optical phase control of nanotunnelling in the single-electron regime. *Nat. Photonics* **10**, 667–670 (2016).
14. P. B. Changala, M. L. Weichman, K. F. Lee, M. E. Fermann, J. Ye, Rovibrational quantum state resolution of the C_{60} fullerene. *Science* **363**, 49–54 (2019).
15. M. Vainio, L. Halonen, Mid-infrared optical parametric oscillators and frequency combs for molecular spectroscopy. *Phys. Chem. Chem. Phys.* **18**, 4266–4294 (2016).

16. M. Quack, J. Stohner, M. Willeke, High-resolution spectroscopic studies and theory of parity violation in chiral molecules. *Annu. Rev. Phys. Chem.* **59**, 741–769 (2008).
17. B. Darquié, C. Stoeffler, A. Shelkovnikov, C. Daussy, A. Amy-Klein, C. Chardonnet, S. Zrig, L. Guy, J. Crassous, P. Soulard, P. Asselin, T. R. Huet, P. Schwerdtfeger, R. Bast, T. Saue, Progress toward the first observation of parity violation in chiral molecules by high-resolution laser spectroscopy. *Chirality* **22**, 870–884 (2010).
18. F. Keilmann, R. Hillenbrand, Near-field microscopy by elastic light scattering from a tip. *Philos. Trans. A Math. Phys. Eng. Sci.* **362**, 787–805 (2004).
19. A. Dazzi, C. B. Prater, AFM-IR: Technology and applications in nanoscale infrared spectroscopy and chemical imaging. *Chem. Rev.* **117**, 5146–5173 (2017).
20. H. A. Bechtel, E. A. Muller, R. L. Olmon, M. C. Martin, M. B. Raschke, Ultrabroadband infrared nanospectroscopic imaging. *Proc. Natl. Acad. Sci. U.S.A.* **111**, 7191–7196 (2014).
21. J. Faist, G. Villares, G. Scalari, M. Rösch, C. Bonzon, A. Hugi, M. Beck, Quantum cascade laser frequency combs. *Nanophotonics* **5**, 272–291 (2016).
22. D. Palaferri, Y. Todorov, A. Bigioli, A. Mottaghizadeh, D. Gacemi, A. Calabrese, A. Vasanelli, L. Li, A. G. Davies, E. H. Linfield, F. Kapsalidis, M. Beck, J. Faist, C. Sirtori, Room-temperature nine-μm-wavelength photodetectors and GHz-frequency heterodyne receivers. *Nature* **556**, 85–88 (2018).
23. H. Pires, M. Baudisch, D. Sanchez, M. Hemmer, J. Biegert, Ultrashort pulse generation in the mid-IR. *Prog. Quantum Electron.* **43**, 1–30 (2015).
24. K. C. Cossel, E. M. Waxman, I. A. Finneran, G. A. Blake, J. Ye, N. R. Newbury, Gas-phase broadband spectroscopy using active sources: Progress, status, and applications. *J. Opt. Soc. Am. B* **34**, 104–129 (2017).
25. S. Maret, A. Faure, E. Scifoni, L. Wiesenfeld, On the robustness of the ammonia thermometer. *Mon. Not. R. Astron. Soc.* **399**, 425–431 (2009).
26. B. Timmer, W. Olthuis, A. van den Berg, Ammonia sensors and their applications—A review. *Sens. Actuators B* **107**, 666–677 (2005).
27. J. Harries, B. Carli, R. Rizzi, C. Serio, M. Mlynczak, L. Palchetti, T. Maestri, H. Brindley, G. Masiello, The far-infrared Earth. *Rev. Geophys.* **46**, 2007RG000233 (2008).
28. A. Baltuška, T. Fuji, T. Kobayashi, Controlling the carrier-envelope phase of ultrashort light pulses with optical parametric amplifiers. *Phys. Rev. Lett.* **88**, 133901 (2002).
29. H. Timmers, A. Kowligy, A. Lind, F. C. Cruz, N. Nader, M. Silfies, G. Ycas, T. K. Allison, P. G. Schunemann, S. B. Papp, S. A. Diddams, Molecular fingerprinting with bright, broadband infrared frequency combs. *Optica* **5**, 727–732 (2018).
30. Q. Wu, X.-C. Zhang, Free-space electro-optics sampling of mid-infrared pulses. *Appl. Phys. Lett.* **71**, 1285–1286 (1997).
31. A. Sell, R. Scheu, A. Leitenstorfer, R. Huber, Field-resolved detection of phase-locked infrared transients from a compact Er:fiber system tunable between 55 and 107 THz. *Appl. Phys. Lett.* **93**, 251107 (2008).
32. A. Bartels, R. Cerna, C. Kistner, A. Thoma, F. Hudert, C. Janke, T. Dekorsy, Ultrafast time-domain spectroscopy based on high-speed asynchronous optical sampling. *Rev. Sci. Instrum.* **78**, 035107 (2007).
33. I. A. Finneran, J. T. Good, D. B. Holland, P. B. Carroll, M. A. Allodi, G. A. Blake, Decade-spanning high-precision terahertz frequency comb. *Phys. Rev. Lett.* **114**, 163902 (2015).
34. R. A. Stead, A. K. Mills, D. J. Jones, Method for high resolution and wideband spectroscopy in the terahertz and far-infrared region. *J. Opt. Soc. Am. B* **29**, 2861–2868 (2012).
35. T. Ideguchi, S. Holzner, B. Bernhardt, G. Guelachvili, N. Picqué, T. W. Hänsch, Coherent Raman spectro-imaging with laser frequency combs. *Nature* **502**, 355–358 (2013).
36. C. Riek, P. Sulzer, M. Seeger, A. S. Moskalenko, G. Burkard, D. V. Seletskiy, A. Leitenstorfer, Subcycle quantum electrodynamics. *Nature* **541**, 376–379 (2017).
37. I. Pupeza, D. Sánchez, J. Zhang, N. Lilienfein, M. Seidel, N. Karpowicz, T. Paasch-Colberg, I. Znakovskaya, M. Pescher, W. Schweinberger, V. Pervak, E. Fill, O. Pronin, Z. Wei, F. Krausz, A. Apolonski, J. Biegert, High-power sub-two-cycle mid-infrared pulses at 100 MHz repetition rate. *Nat. Photonics* **9**, 721–724 (2015).
38. M. Huber, W. Schweinberger, M. Trubetskov, S. A. Hussain, O. Pronin, L. Vamos, E. Fill, A. Apolonski, M. Zigman, F. Krausz, I. Pupeza, Detection sensitivity of field-resolved spectroscopy in the molecular fingerprint region, in *Proceedings of the 2017 Conference on Lasers and Electro-Optics Europe European Quantum Electronics Conference (CLEO/Europe-EQEC)* (IEEE, 2017), p. 1.
39. O. Schubert, M. Hohenleutner, F. Langer, B. Urbanek, C. Lange, U. Huttner, D. Golde, T. Meier, M. Kira, S. W. Koch, R. Huber, Sub-cycle control of terahertz high-harmonic generation by dynamical Bloch oscillations. *Nat. Photonics* **8**, 119–123 (2014).
40. M. F. Ciappina, J. A. Pérez-Hernández, A. S. Landsman, W. A. Okell, S. Zherebtsov, B. Förg, J. Schötz, L. Seiffert, T. Fennel, T. Shaaran, T. Zimmermann, A. Chacón, R. Guichard, A. Zaïr, J. W. G. Tisch, J. P. Marangos, T. Witting, A. Braun, S. A. Maier, L. Roso, M. Krüger, P. Hommelhoff, M. F. Kling, F. Krausz, M. Lewenstein, Attosecond physics at the nanoscale. *Rep. Prog. Phys.* **80**, 054401 (2017).
41. M. Khalil, N. Demirdöven, A. Tokmakoff, Vibrational coherence transfer characterized with Fourier-transform 2D IR spectroscopy. *J. Chem. Phys.* **121**, 362–373 (2004).
42. G. Ycas, F. R. Giorgetta, E. Baumann, I. Coddington, D. Herman, S. A. Diddams, N. R. Newbury, High-coherence mid-infrared dual-comb spectroscopy spanning 2.6 to 5.2 μm. *Nat. Photonics* **12**, 202–208 (2018).
43. A. V. Muraviev, V. O. Smolski, Z. E. Loparo, K. L. Vodopyanov, Massively parallel sensing of trace molecules and their isotopologues with broadband subharmonic mid-infrared frequency combs. *Nat. Photonics* **12**, 209–214 (2018).
44. L. S. Rothman, I. E. Gordon, Y. Babikov, A. Barbe, D. Chris Benner, P. F. Bernath, M. Birk, L. Bizzocchi, V. Boudon, L. R. Brown, A. Campargue, K. Chance, E. A. Cohen, L. H. Coudert, V. M. Devi, B. J. Drouin, A. Fayt, J.-M. Flaud, R. R. Gamache, J. J. Harrison, J.-M. Hartmann, C. Hill, J. T. Hodges, D. Jacquemart, A. Jolly, J. Lamouroux, R. J. Le Roy, G. Li, D. A. Long, O. M. Lyulin, C. J. Mackie, S. T. Massie, S. Mikhailenko, H. S. P. Müller, O. V. Naumenko, A. V. Nikitin, J. Orphal, V. Perevalov, A. Perrin, E. R. Polovtseva, C. Richard, M. A. H. Smith, E. Starikova, K. Sung, S. Tashkun, J. Tennyson, G. C. Toon, V. G. Tyuterev, G. Wagner, The HITRAN2012 molecular spectroscopic database. *J. Quant. Spectrosc. Radiat. Transfer* **130**, 4–50 (2013).
45. I. Coddington, N. Newbury, W. Swann, Dual-comb spectroscopy. *Optica* **3**, 414–426 (2016).
46. V. Nemtchinov, K. Sung, P. Varanasi, Measurements of line intensities and half-widths in the 10-μm bands of $^{14}NH_3$. *J. Quant. Spectrosc. Radiat. Transfer* **83**, 243–265 (2004).
47. W. Demtroder, *Molecular Physics: Theoretical Principles and Experimental Methods* (Wiley Interscience, ed. 1, 2005).
48. J. L. Bohn, A. M. Rey, J. Ye, Cold molecules: Progress in quantum engineering of chemistry and quantum matter. *Science* **357**, 1002–1010 (2017).
49. E. A. Muller, B. Pollard, H. A. Bechtel, P. van Blerkom, M. B. Raschke, Infrared vibrational nanocrystallography and nanoimaging. *Sci. Adv.* **2**, e1601006 (2016).
50. D. R. Carlson, D. D. Hickstein, W. Zhang, A. J. Metcalf, F. Quinlan, S. A. Diddams, S. B. Papp, Ultrafast electro-optic light with subcycle control. *Science* **361**, 1358–1363 (2018).
51. K. Lee, J. Lee, Y.-S. Jang, S. Han, H. Jang, Y.-J. Kim, S.-W. Kim, Fourier-transform spectroscopy using an Er-doped fiber femtosecond laser by sweeping the pulse repetition rate. *Sci. Rep.* **5**, 15726 (2015).
52. M. J. Baker, E. Gazi, M. D. Brown, J. H. Shanks, P. Gardner, N. W. Clarke, FTIR-based spectroscopic analysis in the identification of clinically aggressive prostate cancer. *Br. J. Cancer* **99**, 1859–1866 (2008).
53. M. J. Baker, J. Trevisan, P. Bassan, R. Bhargava, H. J. Butler, K. M. Dorling, P. R. Fielden, S. W. Fogarty, N. J. Fullwood, K. A. Heys, C. Hughes, P. Lasch, P. L. Martin-Hirsch, B. Obinaju, G. D. Sockalingum, J. Sulé-Suso, R. J. Strong, M. J. Walsh, B. R. Wood, P. Gardner, F. L. Martin, Using fourier transform IR spectroscopy to analyze biological materials. *Nat. Protoc.* **9**, 1771–1791 (2014).
54. Y. Gokarn, S. Agarwal, K. Arthur, A. Bepperling, E. S. Day, D. Filoti, D. G. Greene, D. Hayes, R. Kroe-Barrett, T. Laue, J. Lin, B. McGarry, V. Razinkov, S. Singh, R. Taing, S. Venkataramani, W. Weiss, D. Yang, I. E. Zarraga, *State-of-the-Art and Emerging Technologies for Therapeutic Monoclonal Antibody Characterization Volume 2. Biopharmaceutical Characterization: The NISTmAb Case Study*, vol. 1201 of *ACS Symposium Series* (American Chemical Society, 2015), pp. 285–327.
55. E. A. Muller, B. Pollard, H. A. Bechtel, R. Adato, D. Etezadi, H. Altug, M. B. Raschke, Nanoimaging and control of molecular vibrations through electromagnetically induced scattering reaching the strong coupling regime. *ACS Photonics* **5**, 3594–3600 (2018).
56. B. Wolter, M. G. Pullen, M. Baudisch, M. Sclafani, M. Hemmer, A. Senftleben, C. D. Schröter, J. Ullrich, R. Moshammer, J. Biegert, Strong-field physics with mid-IR fields. *Phys. Rev. X* **5**, 021034 (2015).
57. S. A. Diddams, L. Hollberg, V. Mbele, Molecular fingerprinting with the resolved modes of a femtosecond laser frequency comb. *Nature* **445**, 627–630 (2007).
58. C. Riek, D. V. Seletskiy, A. Leitenstorfer, Femtosecond measurements of electric fields: From classical amplitudes to quantum fluctuations. *Eur. J. Phys.* **38**, 024003 (2017).
59. A. Leitenstorfer, S. Hunsche, J. Shah, M. C. Nuss, W. H. Knox, Detectors and sources for ultrabroadband electro-optic sampling: Experiment and theory. *Appl. Phys. Lett.* **74**, 1516–1518 (1999).
60. C. Riek, D. V. Seletskiy, A. S. Moskalenko, J. F. Schmidt, P. Krauspe, S. Eckart, S. Eggert, G. Burkard, A. Leitenstorfer, Direct sampling of electric field vacuum fluctuations. *Science* **350**, 420–423 (2015).
61. R. R. Gamache, Lineshape paramteres for water vapor in the 3.2–17.76 μm region for atmospheric applications. *J. Mol. Spectrosc.* **229**, 9–18 (2005).

Acknowledgments: We thank J. E. Schiel and T. Mouchahoir for providing the NISTmAb samples and D. Lesko for providing the NH_3 lecture bottle sample. We thank N. Newbury, D. Carlson, K. Cossel, M. Weichman, and C. Meuse for providing comments on the manuscript. We thank A. Bartels for advice on the experimental setup. **Funding:** This work was supported by the Defense Advanced Research Projects Agency (DARPA), National Institute of Standards and Technology (NIST), National Research Council (NRC/National Academies of Sciences, Engineering, and Medicine), and Air Force Office of Scientific Research (AFOSR) (FA9550-16-1-0016). F.C.C. acknowledges funding from Fapesp (grant # 2018/26673-5). U.E. and J.B. acknowledge funding from "Severo Ochoa" Programme for Centres of Excellence in R&D (SEV-2015-0522), MINECO "FIS2017-89536-P", AGAUR "2017 SGR 1639", EU FET "PETACom" (829153), ERC Advanced Grant "TRANSFORMER" (788218) and PoC miniX (840010).

Author contributions: A.S.K., H.T., A.J.L., and U.E. performed the experiment and collected the data. A.S.K., H.T., A.J.L., F.C.C., and S.A.D. developed the frequency control and locking electronics. P.G.S. provided the OP-GaP nonlinear crystal. A.S.K., H.T., A.J.L., F.C.C., J.B., and S.A.D. conceived the concept and its implementation. All authors contributed to the writing of the manuscript and discussion of the results. **Competing interests:** The authors declare that they have no competing interests. **Data and materials availability:** All data needed to evaluate the conclusions in the paper are present in the paper and/or the Supplementary Materials. Additional data related to this paper may be requested from the authors.

Submitted 1 February 2019
Accepted 2 May 2019
Published 7 June 2019
10.1126/sciadv.aaw8794

Citation: A. S. Kowligy, H. Timmers, A. J. Lind, U. Elu, F. C. Cruz, P. G. Schunemann, J. Biegert, S. A. Diddams, Infrared electric field sampled frequency comb spectroscopy. *Sci. Adv.* **5**, eaaw8794 (2019).

Infrared electric field sampled frequency comb spectroscopy

Abijith S. Kowligy, Henry Timmers, Alexander J. Lind, Ugaitz Elu, Flavio C. Cruz, Peter G. Schunemann, Jens Biegert and Scott A. Diddams

Sci Adv **5** (6), eaaw8794.
DOI: 10.1126/sciadv.aaw8794